Chem. Res. Chin. Univ., 2018, 34(4), 635—642 doi: 10.1007/s40242-018-7381-1

Preparation and Characterization of SiO_2/Co and C/Co Nanocomposites as Fisher-Tropsch Catalysts for CO_2 Hydrogenation

HAN Fuqin[1], ZHANG Zhe[1], NIU Na[2*] and LI Jian[1]

1. College of Science, Northeast Forestry University, Harbin 150040, P. R. China;
2. Key Laboratory of Bio-based Material Science and Technology, Ministry of Education, Northeast Forestry University, Harbin 150040, P. R. China

Abstract To fabricate high-density cobalt-based catalysts, we first synthesized SiO_2/C composites *via* a hydrothermal method and removed C and SiO_2 by two different methods, respectively. The as-prepared SiO_2 and C supports then reacted with cobalt acetylacetonate and *N,N*-dimethylformamide(DMF) under hydrothermal conditions to prepare SiO_2/Co and C/Co nanocomposite catalysts. The catalysts were characterized by X-ray diffraction(XRD), scanning electron microscope(SEM), transmission electron microscopy(TEM), inductively coupled plasma mass spectrometry(ICP), energy dispersive X-ray fluoresence spectrometer(EDX), and nitrogen adsorption. It was found that hexagonal cobalt nanocrystals were successfully integrated with the mesoporous silica or carbon nanotube supports. SEM and TEM results show that SiO_2/Co composites with a hollow/mesoporous sphere structure and C/Co composites with a tubular structure have been successfully synthesized. Both composite samples show superparamagnetism exhibiting an S-type hysteresis loop, which originated from the cobalt nanoparticles in the samples. Nitrogen adsorption/desorption curves suggest that the SiO_2 and C supports have well-developed pore structures and large specific surface areas, and the loading and good dispersity of cobalt nanoparticles on the supports were proven by ICP and EDX. Moreover, the samples exhibited good and stable catalytic activity, demonstrating that the two composites are suitable catalysts for Fischer-Tropsch CO_2 hydrogenation.

Keywords Mesoporous SiO_2; Carbon nanotube; Cobalt based catalyst; Fischer-Tropsch reaction; CO_2 hydrogenation

1 Introduction

Coal or natural gas can be converted to engine fuel by a Fischer-Tropsch(F-T) synthesis process, which refers to the synthesis of hydrocarbons and oxygen using crude syngas obtained by coal vaporization under the action of a catalyst in a reactor[1—3]. In fact, F-T synthesis is a complicated process, whose products comprise high-quality liquid fuels and chemicals(no sulfur, nitrogen, or metals, and low aromatic content) obtained by desulphurization, deoxidization, and adjustment of the hydrogen/carbon ratio in the syngas, followed by further refining and cracking[4,5]. Previous studies have shown that both CO and CO_2 can be used in catalytic hydrogenation reactions under F-T synthesis conditions, but the selectivity and distribution of the resulting products are quite different[6—8]. The hydrogenation of CO leads to the formation of many high-molecular-weight products[9], whereas CO_2 hydrogenation gives rise to gaseous products(easy capture and storage)[10,11]. With the global increase in population and acceleration of industrialization, the amount of CO_2 emission is increasing, which causes serious environmental problems, such as the greenhouse effect, global warming, and the thermal island effect. However, CO_2 can be considered as a double-edged sword with advantages as well as shortcomings. As CO_2 is one of the most abundant carbon resources, the environmental problems and energy issues could be solved if we could utilize CO_2 effectively[12].

It is particularly important to develop catalysts with high activity and selectivity for the F-T synthesis process. It has been shown that this process can be catalyzed by certain transition metals, such as Cu[13,14], Ni[15,16], Rh[17,18], Fe[19,20], and Co[21,22]. Among these catalysts, cobalt-based catalysts exhibit relatively high CO_2 hydrogenation activity, chain growth ability, and CO_2 conversion rate, which makes them suitable for reaction systems with higher hydrogen/carbon ratios[23]. Furthermore, the hydrogenation process employing cobalt-based catalysts is relatively stable, with high selectivity for heavy straight-chain saturated hydrocarbons and long service life[24,25]. Therefore, cobalt-based catalysts have received widespread attention from researchers with the aim of applying them in

*Corresponding author. Email: niuna@nefu.edu.cn

Received November 28, 2017; accepted April 26, 2018.

Supported by the Natural Science Foundation of Heilongjiang Province, China(No.B20170001), the Postdoctoral Fund of Heilongjiang Province, China(No.LBH-Z16009), the Fundamental Research Funds for the Central Universities, China(No. 2572018BC28) and the Postdoctoral Science Foundation of China(Nos.2016M591501, 2017T100218).

actual production. Generally, for Co-based catalysts, there are many kinds of supports including insulating oxides, semiconducting oxides, and metals. SiO_2[26,27], Al_2O_3[28,29], TiO_2[30,31], ZrO_2[32,33], mesoporous carbon[34,35], and carbon nanotubes[36,37] have been reported for the use as supports for Co-based catalysts. Among these, mesoporous SiO_2 and carbon nanotubes are two kinds of excellent supports; however, the related research is very limited, especially for carbon nanotube-supported cobalt catalysts. Mesoporous SiO_2 possesses high specific surface area, ordered pore structure, narrow pore size distribution, and adjustable aperture size[38,39], which can improve the dispersity of metal particles, thus enhancing the catalytic activity and thermal stability of the catalyst[40,41]. The surface of SiO_2 is rich in hydroxyl silicon, whose distribution, concentration, and nature have a great influence on the dispersion and reduction degree of loaded cobalt catalysts[42]. Carbon nanotubes have been applied for the preparation of cobalt-based catalysts in recent years because of their high purity, good mechanical properties, high thermal conductivity, and large specific surface area[43—45]. As supports for catalysts, an interesting trait of carbon nanotubes is that there exists a weak interaction between cobalt and carbon nanotubes, which prevents the formation of reducing species and results in the modifiability on the surface of carbon nanotubes, providing the possibility for preparation of highly dispersed cobalt catalysts[46,47].

Herein, two-dimensional C/Co nanotube composite and hollow/mesoporous SiO_2/Co composite materials were successfully synthesized through a two-step process. Firstly, mesoporous SiO_2 and carbon nanotubes were obtained by removing carbon and SiO_2, respectively, in synthesized SiO_2/C composites. Subsequently, cobalt crystals were bonded to the as-prepared supports through a hydrothermal process using $Co(acac)_2$ as a precursor. The structures and catalytic properties of the composites were investigated by a series of characterization experiments. The results demonstrate that hexagonal cobalt nanocrystals have been successfully loaded on the mesoporous SiO_2 or carbon nanotube supports, and the SiO_2/Co composites with a hollow/mesoporous structure and the C/Co composites with a tubular structure have been obtained with diameters of approximately 400 and 50 nm, respectively. The SiO_2/Co and C/Co composite catalysts exhibited appropriate aperture size and pore volume as well as large surface area, resulting in excellent catalytic activity and stability during F-T CO_2 hydrogenation, which will be conducive to potential applications of the catalysts in actual production processes.

2 Experimental

2.1 Materials

All chemical reagents used in our experiments were purchased from Sigma-Aldrich and were of analytical grade, used without further purification.

2.2 Synthesis of Mesoporous SiO_2 and C Nanotube Supports

Firstly, 0.2 mL of 25% NH_3 H_2O(ammonia solution) was mixed with 0.2 g of resorcinol. For the preparation of SiO_2 support, 28 mL of ethanol and deionized water mixture solution with various volume ratios(8/20, 12/16, and 16/12) was then added; for the preparation of C nanotube support, 28 mL of ethanol and deionized water mixture solution with a volume ratio of 4/24 was added. Then, the mixture was stirred for 30 min, and 0.28 mL of methanol was added dropwise to the mixture. After further stirring for 5 min, 1 mL of tetraethylsilicate(TEOS) and 0.1 g of cetyltrimethylammonium bromide (CTAB) were slowly added to the solution with continuous stirring. After stirring for another 1 h, the solution was transferred into a muffle oven and annealed at 80 °C for 24 h. After centrifugation, washing, and drying, the obtained sample was transferred into a crucible and put in a muffle oven at 600 °C for 3 h under N_2 atmosphere, and the composite material was obtained and denoted as SiO_2/C. To obtain mesoporous SiO_2, the SiO_2/C composite was calcined for 5 h in air to remove C; to obtain C nanotubes, the SiO_2/C composite was dipped in 2 mol/L sodium hydroxide (NaOH) solution to remove SiO_2.

2.3 Synthesis of SiO_2/Co and C/Co Nanocomposites

For both SiO_2/Co and C/Co composites, Co nanocrystals were synthesized by using *N,N*-dimethylformamide(DMF) as the solvent and $Co(acac)_2$ as cobalt precursor. To synthesize SiO_2/Co composites, the above mesoporous SiO_2 sample was added to 30 mL of nitric acid(HNO_3) aqueous solution (3 mmol/L), and the mixture was stirred for 2 h. Then, 0.026 g of $Co(acac)_2$ and 30 mL of DMF were added to the mixture. After stirring for 1 h, the mixture was transferred into a muffle oven and annealed at 200 °C for 12 h. After centrifugation, washing with water and ethanol, and drying at 60 °C, the sample was collected and denoted as SiO_2/Co. Similarly, to synthesize C/Co composites, the carbon nanotubes obtained above were added to 0.026 g of $Co(acac)_2$ and 30 mL of DMF. After stirring for 30 min, the mixture was transferred into a muffle oven and annealed at 200 °C for 12 h. After centrifugation, washing with water and ethanol twice, and drying at 60 °C, the resulting sample was collected and denoted as C/Co.

2.4 Characterizations

X-Ray diffraction(XRD) measurements were carried out on a D/max-2200VPC powder X-ray diffractometer(Rigaku Corp., Tokyo, Japan) with Cu $K\alpha$ radiation(40 kV, 40 mA). The morphologies of the catalysts and their precursors were observed on a JEOL JXA-840 scanning electron microscope (SEM) instrument operating at 20 kV. Transmission electron microscopy (TEM) and high-resolution transmission electron microscopy (HRTEM) measurements were performed on a JEM 2100 transmission electron microscope(JEOL Ltd., Tokyo, Japan) at an accelerating voltage of 200 kV to elucidate the dimensions and structural details of the samples. The microscopic morphologies and structures of the as-synthesized samples were investigated by field emission scanning electron microscopy(FESEM, S4800, Hitachi, Japan) and energy-

dispersive X-ray spectroscopy(EDS, JEOL JXA-840). The elemental content of the sample was evaluated by inductively coupled plasma atomic emission spectrometry(ICP-AES, Optima 8300). The Brunauer-Emmett-Teller(BET) surface area, average pore diameter, and pore volume data were obtained by nitrogen physisorption measurements using a Quantachrome Nova 2000 automated system(USA). The magnetic properties of the samples were measured on an MPMS-XL-7 superconducting quantum interference magnetometer.

2.5 Determination of Cobalt Content(ICP)

For the SiO_2/Co catalyst, 1.5 g of dry catalyst was dissolved in hydrofluoric acid(HF). After the catalyst was completely dissolved, hydrochloric acid(HCl) was added to the solution. The resulting solution was diluted with water and made up to the required volume for testing.

For the C/Co catalyst, 1.3 g of dry catalyst was dissolved in HCl. The precipitated carbon was removed by centrifugation, and the remaining solution was diluted with water and measured.

2.6 Catalytic Characterization

CO_2 hydrogenation reactions over the SiO_2- and C-supported cobalt catalysts were performed using a steel tubular plug flow reactor. For the tests, 50 mg of the catalyst sample was loaded between the plugs of quartz wool with a K-thermocouple monitoring the reactor temperature. Firstly, the samples were reduced at 400 °C for 30 min under a H_2 flow of 50 mL/min. Then, the chamber temperature was decreased to the reaction temperature. At the same time, a feed mixture containing H_2, CO_2, and Ar(Ar was the internal standard to ensure accurate mass balances) was used in the purifying traps to remove all other impurities. The purified mixture was then passed through the catalyst at a flow rate of 60 mL/min with $n(H_2):n(CO_2):n(Ar)=4:1:0.5$. The individual flow rates were maintained using separate mass flow controllers(Bronkhorst). After 0.5 h, all the products in the reactor including unconverted reactants were sent to a hot vessel heated at 110 °C to collect liquid aqueous and organic products. The non-condensable gases were depressurized by means of electronic back pressure(Brooks Instrument Mod. 5866) and totalized on a flow gas meter(Ritter Mod. TG05-5). Then, the gas flow was introduced into a gas chromatography equipment (GC-14C, Shimadzu). Blank experiments were also conducted under the same reaction conditions with the flow of reactants H_2 and CO_2.

3 Results and Discussion

3.1 Synthesis and Characterization of the Materials

XRD patterns of the as-synthesized SiO_2 support, SiO_2/Co composite, C support, and C/Co composite are presented in Fig.1. In Fig.1(A), a broad diffraction peak at 2θ=22° can be observed, which is indexed to pure amorphous SiO_2(JCPDS Card No. 29-0085). As the SiO_2/Co composite was prepared by using DMF as the solvent and $Co(acac)_2$ as the precursor, besides a broad diffraction peak corresponding to amorphous SiO_2, the XRD pattern also shows the characteristic sharp peaks of Co(JCPDS Card No. 15-0806), confirming the successful synthesis of SiO_2/Co composites. Fig.1(B) shows a characteristic peak at 2θ of 25° for the prepared C support. After loading Co, we can see the presence of two diffraction peaks corresponding to C and Co in the C/Co composite, which indicates successful loading of Co nanoparticles on C nanotubes. However, the intensity of the peak at 2θ=25° is reduced markedly, probably due to partial burning of C nanotubes when calcined at 600 °C for 5 h in an air atmosphere.

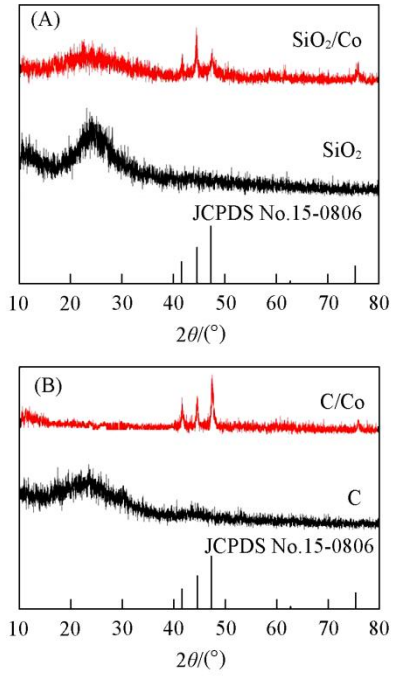

Fig.1 XRD patterns of SiO_2, SiO_2/Co composite(A) and C, C/Co composite(B)

The standard date lines of Co(JCPDS No.15-0806) are given for comparison.

SEM, TEM, and HRTEM measurements of the support materials as well as support/Co composites were performed, and the results are shown in Figs.2 and 3. As can be seen from Fig.2(A), a tubular carbon support was obtained, and the size of the carbon support materials ranges from nanometers to micrometers with a diameter of about 50 nm. TEM images of the C support are present in Fig.2(B), which show that many nanotubes mutually intertwine, and the corresponding enlarged image(inset) suggests that C nanotubes exhibit 2D bending to some extent, whose seal at the top is circular. Fig.3(A) indicates that cobalt loading does not change the tubular structure of the C support; the fluffy structure on the surface of the support is considered to be Co nanoparticles with a relatively uniform size. At the same time, the loading of cobalt on the support was investigated by ICP. We found that the actual loading was 2.87%(mass fraction), which is very close to the theoretical loading of 3%, indicating that cobalt was successfully loaded on the C support. The dispersity of cobalt nanoparticles was further investigated by scanning transmission electron microscopy(STEM) image and EDS elemental mapping.

Fig.3(E)—(G) show the EDS mapping of cobalt, carbon, and oxygen element on region of C/Co composite TEM image, and the mapping of Co suggests that the cobalt nanoparticles are uniformly dispersed on the carbon nanotubes. TEM and HRTEM images of the C/Co composite are shown in Fig.3(B) and (C), in which notable lattice fringes are distinguishable from the image, and the lattice spacing of the C/Co catalyst is 0.2162 nm, corresponding to the (111) plane of the hexagonal phase of Co, which reveals the high crystallinity and dispersity of the sample.

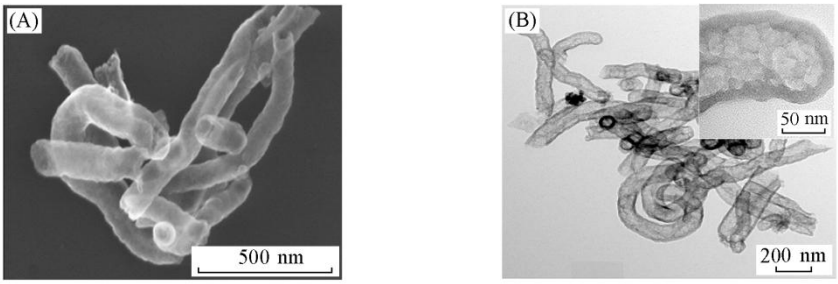

Fig.2 SEM(A) and TEM(B) images of C support
Inset of (B): the corresponding enlarged image.

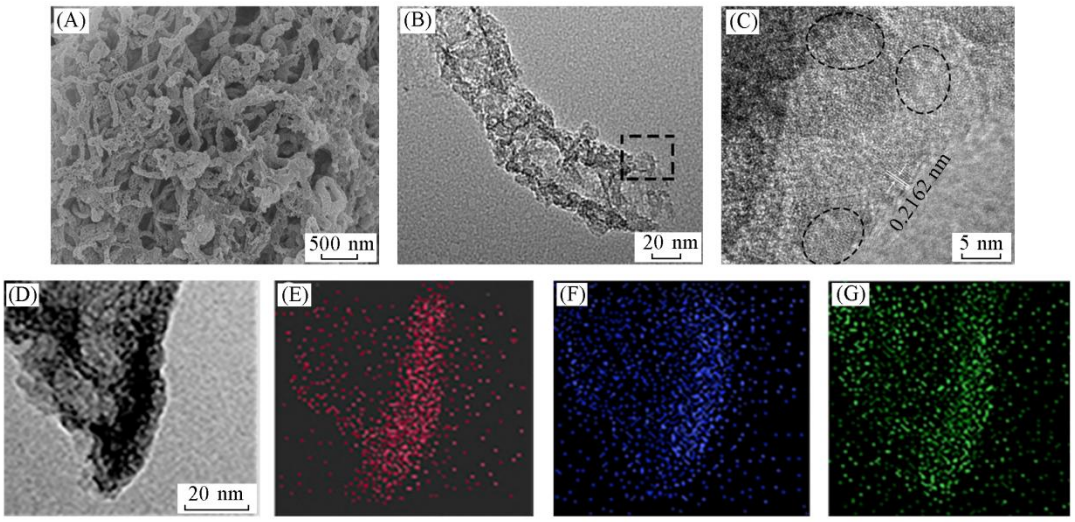

Fig.3 SEM(A), TEM(B), HRTEM(C) and STEM(D) images and EDS elemental mapping(E—G) of C/Co composite
The dotted lines in (C) show the lattice fringes. (E) Co; (F) C; (G) O.

For the SiO_2 support, as shown in Figs.4 and 5, we can observe the reunion of the obtained SiO_2 sample when $V(C_2H_5OH)/V(H_2O)$=8/20[Fig.4(A)], and when $V(C_2H_5OH)/V(H_2O)$=16/12[Fig.4(B)], some SiO_2 spheres are broken. Therefore, we chose SiO_2 prepared with $V(C_2H_5OH)/V(H_2O)$= 12/16 for the following measurements[Fig.4(C)]. Fig.4(C) displays the SEM image, which suggests that spherical SiO_2 particles of regular shape and uniform size were prepared. The high-magnification SEM image in the inset of Fig.4(C) shows that the SiO_2 support has an obvious hollow/mesoporous structure with the diameter ranging from 400 nm to 500 nm. Fig.5(A) shows a representative SEM image of the SiO_2/Co composite, from which we can also conclude that the fluffy structure on the SiO_2 surface originates from the Co nanocrystals. According to the ICP measurement results, the actual loading of 2.36% is close to the theoretical loading of 2.4%, which indicates that cobalt was successfully loaded on the SiO_2 support. The dispersity of Co nanoparticles was investigated by TEM image and EDS elemental mapping. The EDS mapping of Co element on the region of the TEM image of SiO_2/Co

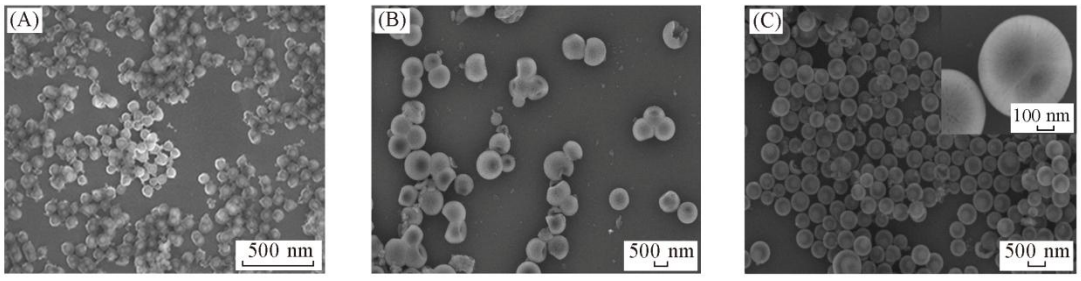

Fig.4 SEM images of SiO_2 support with $V(C_2H_5OH)/V(H_2O)$ of 8/20(A), 16/12(B) and 12/16(C)
Inset of (C): enlarged image.

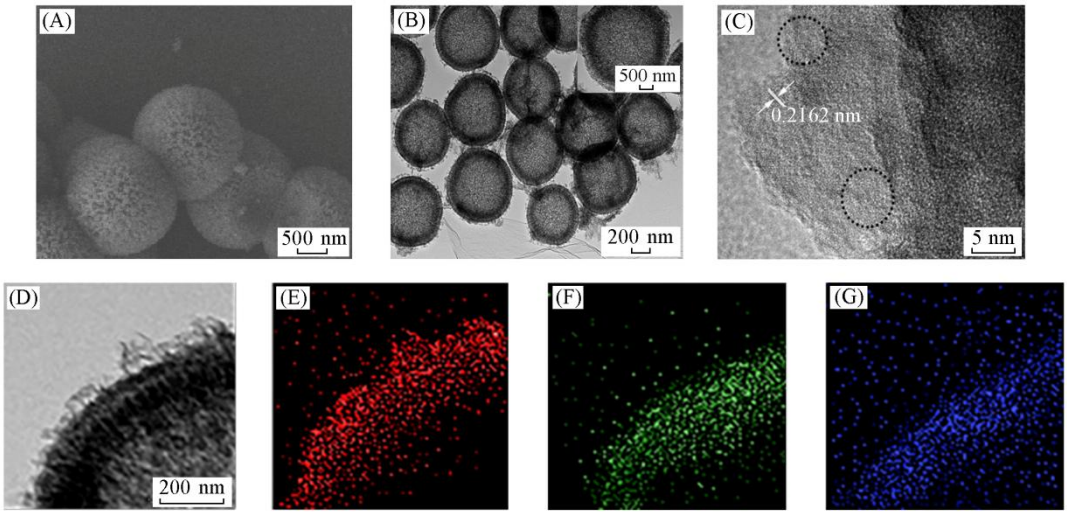

Fig.5 SEM(A), TEM(B), HRTEM(C) and STEM(D) images and EDS elemental mapping(E—G) of SiO_2/Co composite

The dotted lines in (C) show the lattice fringes. Inset of (B): enlarged image. (E) Co; (F) Si; (G) O.

composite in Fig.5(D) indicates a good dispersity of cobalt nanoparticles on the mesoporous SiO_2. According to the TEM image shown in Fig.5(B), the SiO_2/Co composite also has a regular shape, uniform size, and good dispersion. Similar to the C/Co composite, obvious lattice planes can be observed in the HRTEM image[Fig.5(C)], and the corresponding interplanar spacing was about 0.2162 nm, which is consistent with the $d_{(111)}$ spacing of Co(JCPDS Card No.15-0806). The agglomeration phenomenon of Co nanoparticles on the SiO_2 surface was not evident, but some Co particles existed in the mesoporous structure of SiO_2, which implies that the pore structure may be partly blocked. The formation mechanisms of the SiO_2/Co and C/Co composites are alike, showing that metal cations can combine with O atoms through electrostatic forces, where the O atom originates from oxygen-containing functional groups, such as carboxyl and hydroxyl groups on the SiO_2 and C surfaces. In this experiment, cobalt acetylacetonate, whose chelating key is relatively stable, acts as the source of Co^{2+}, but separation will occur at certain pH or high temperature, and a large number of Co^{2+} ions are isolated from cobalt acetylacetonate when the reaction proceeds under hydrothermal conditions at 220 °C. The isolated Co^{2+} ions are then attracted by the oxygen-containing functional groups on the modified SiO_2 and C surfaces, which greatly contribute to the formation process of the final Co nanocrystals. Scheme 1 clearly demonstrates the formation process of the SiO_2/Co and C/Co composites.

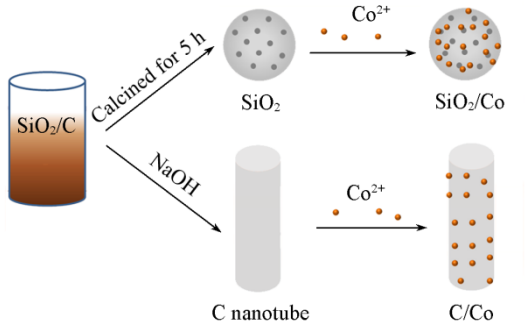

Scheme 1 Formation process of SiO_2/Co and C/Co nanocomposites

Owing to the existence of Co nanoparticles, we also investigated the magnetic properties of the C/Co and SiO_2/Co composites. Fig.6 shows that the saturation magnetization values of C/Co and SiO_2/Co are 3.4 and 3.0 A m^2/kg, respectively. In general, the magnetic hysteresis loops confirm the magnetic features of samples. As shown in Fig.6, the magnetization hysteresis loops are S-like curves; therefore, the as-prepared catalysts possess unique superparamagnetic characteristics, which means that the composite will have no remaining magnetism when the external magnetic field is removed, and the superparamagnetism of cobalt itself will have no undesirable effect on the catalyst.

Fig.7 presents the N_2 adsorption/desorption isotherms of

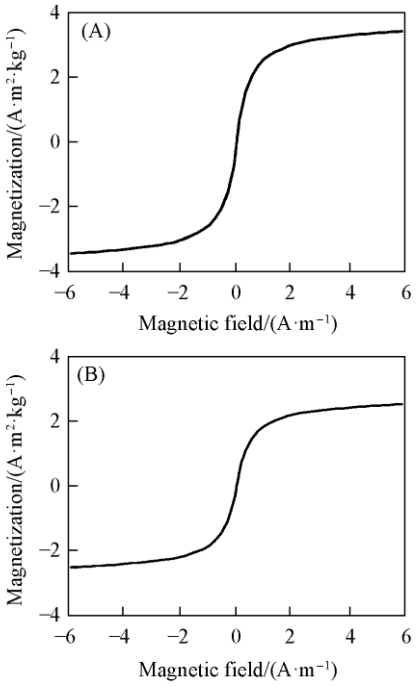

Fig.6 Magnetic hysteresis loops of C/Co(A) and SiO_2/Co catalysts(B)

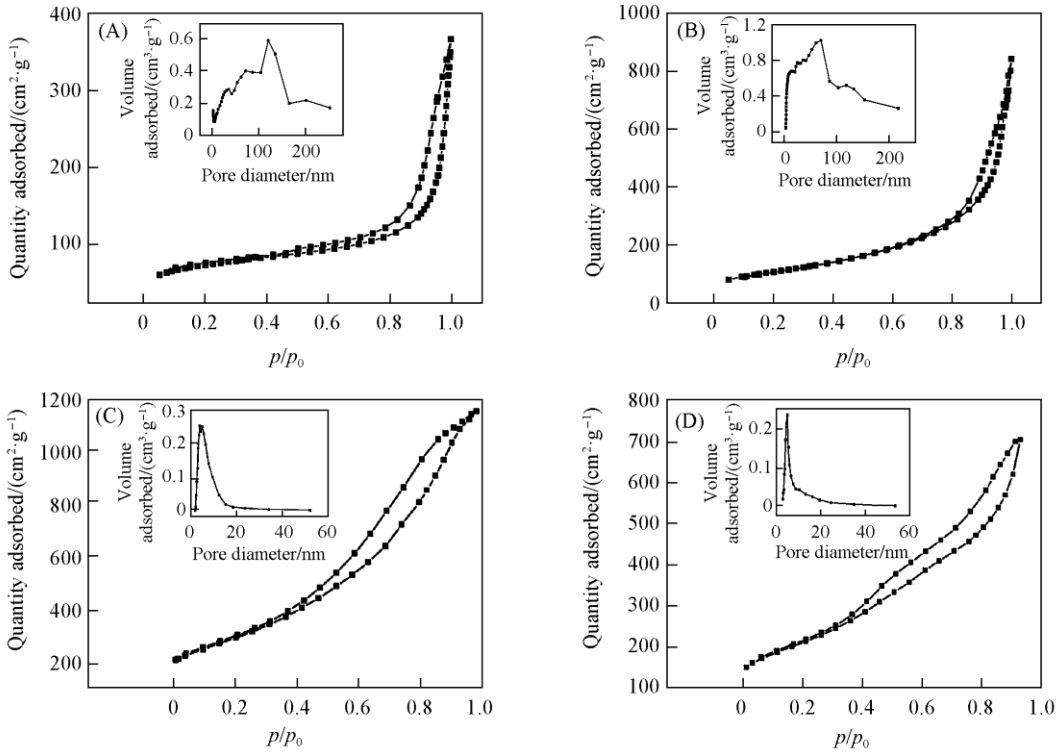

Fig.7 N_2 adsorption-desorption isotherms and size distribution(insets) of SiO_2 support(A), SiO_2/Co composite(B), C support(C) and C/Co composite(D)

SiO_2[Fig.7(A)] and SiO_2/Co[Fig.7(B)]. The BET surface area of the SiO_2 support is 384.1049 m^2/g, the pore volume is 1.270847 cm^3/g, and the average pore size is 13.9974 nm, indicating that the hollow/mesoporous SiO_2 support has a large surface area and suitable pore size, which will be beneficial to the catalytic performance. After reacting with Co, the BET surface area, pore volume, and average pore size of SiO_2/Co are decreased to 243.9024 m^2/g, 0.487785 cm^3/g, and 12.7515 nm, respectively. Clearly, the average pore size does not change much after Co loading, but the surface area and pore volume decrease significantly, which may be caused by the blockage of some small pores of SiO_2 support by Co after loading and roasting. It can be found that the adsorption amount is related to the relative pressure; the adsorption amount increases with increasing the relative pressure from 0 to 0.8, suggesting that a larger relative pressure is beneficial to the adsorption. The adsorption volume increases first and then decreases with increasing pore diameter, reaching a maximum when the pore size is about 125 nm. This result provides an evidence for the successful synthesis of SiO_2/Co catalysts.

Equally, the N_2 adsorption/desorption isotherms of C and C/Co are shown in Fig.7(C) and (D). After Co loading, the BET surface area is decreased from 982 m^2/g to 722 m^2/g, the pore volume is decreased from 1.270847 cm^3/g to 1.06 cm^3/g, and the average pore size is decreased from 8 nm to 5 nm. The decreases here are mainly due to the filling of holes inside the C support by cobalt particles, which greatly reduces the catalyst specific surface area; another possible reason is that some cobalt particles may be loaded on the ends of the carbon nanotubes, which decreases the specific surface area of carbon nanotubes.

3.2 Catalytic Analysis of C/Co and SiO_2/Co Composites

CO_2 hydrogenation reactions over the C- and SiO_2-supported cobalt catalysts were performed on a steel tubular plug. An illustration of the catalytic reaction device is shown in Scheme 2. The catalyst sample(50 mg) was loaded between the plugs of quartz wool and high-purity H_2 and CO_2 were passed through the catalyst. The reactor temperature was controlled by a K-thermocouple and visually monitored by a computer equipped with software. To evaluate the relation between catalytic performance and temperature, CO_2 conversion(%) was calculated at different automatically adjusted temperatures. In addition, the catalytic stabilities of the catalysts over prolonged times at certain temperatures were studied.

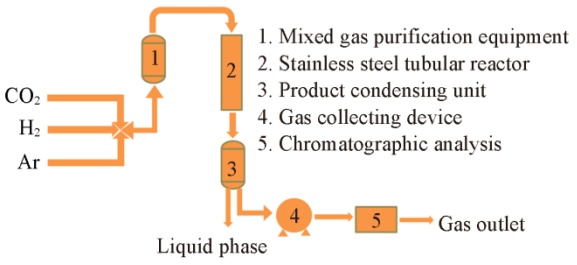

Scheme 2 Catalytic reaction installation diagram of SiO_2/Co and C/Co catalysts

The catalyst bed was flushed with a downward flow of H_2 and CO_2 at a certain temperature. The liquid phase components of reaction products comprised hydrocarbons, paraffin, and

olefins, and the gas phase components comprised mainly CH_4 as well as unreacted H_2, CO_2, and Ar. The mixed gas was introduced into a gas chromatography instrument to analyze the composition. The CO_2 conversion(%) was calculated using the following equation:

$$CO_2(\%) = \left[\frac{n(CO_{2,in}) - n(CO_{2,out}) \times \text{Gas contraction}}{n(CO_{2,in})}\right] \times 100\%$$

where $n(CO_{2,in})$ represents the amount of substance of introduced CO_2, and the concentration of $CO_{2,out}$ gas[$n(CO_{2,out})$] was calibrated by Ar_{in}/Ar_{out}.

Fig.8(A) shows that the CO_2 conversions of the C/Co catalysts at 200, 250 and 300 °C calculated using the above equation are 3%, 9%, and 12%, respectively. It is clear that the CO_2 conversion increases gradually with increasing reaction temperature, indicating that the catalytic activity increases with increasing temperature. According to Fig.8(B), the CO_2 conversion is 11% when the number of cycles is one, and the conversion remains above 10% even when the number of cycles is increased to eight, indicating excellent catalytic stability of the catalysts. The excellent activity and stability of the C/Co catalyst may be related to the loading capacity and dispersion of Co metal on the catalyst surface, which is consistent with the SEM and ICP results above.

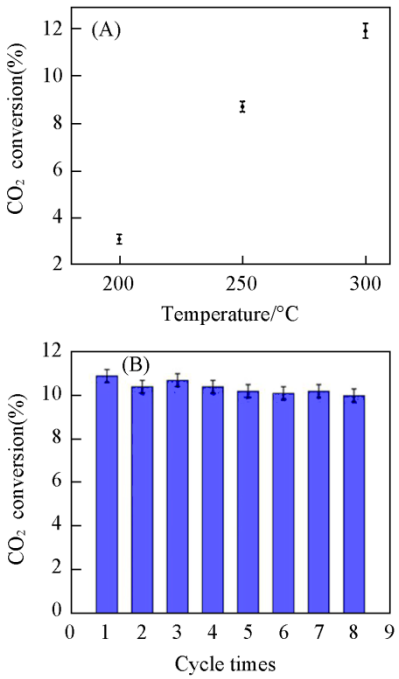

Fig.8 Catalysis activities of the C/Co composites prepared at 200, 250 and 300 °C for CO_2 hydrogenation reactions(A) and catalytic stability properties of the C/Co composites prepared at 200 °C(B)

Fig.9(A) shows that the CO_2 conversions of the SiO_2/Co catalysts at 200, 250 and 300 °C calculated using the equation are 2%, 8%, and 11%, respectively. As shown in Fig.9(B), the CO_2 conversion is 11% when the number of cycles is one, and the conversion remains above 9% even when the number of cycles is increased to eight. Therefore, the SiO_2/Co catalyst possesses good activity and stability. Here, the catalytic activity of cobalt-based catalysts is directly proportional to the loading of cobalt metal on the surface of the catalysts.

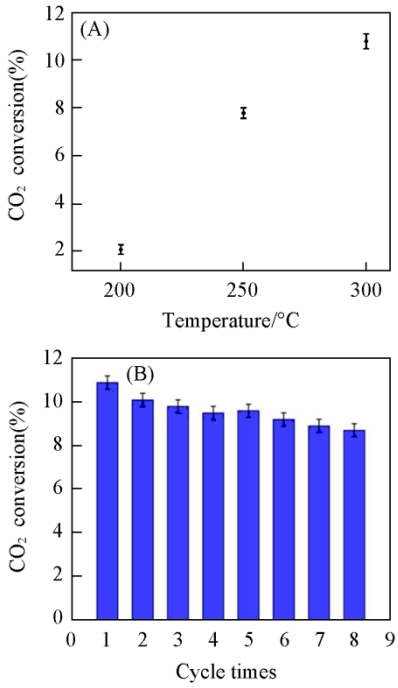

Fig.9 Catalysis activities of the SiO_2/Co composites prepared at 200, 250, and 300 °C for CO_2 hydrogenation reactions(A) and catalytic stability properties of the SiO_2/Co composites prepared at 200 °C(B)

4 Conclusions

SiO_2/Co composites with a mesoporous structure and C/Co composites with a 2D nanotube structure exhibiting large specific surface area and strong adsorption ability were successfully synthesized, which showed excellent catalytic activity in F-T CO_2 hydrogenation. Moreover, it was found that the loading and dispersibility of Co nanoparticles on the catalyst surface greatly affected the catalytic activity, and the Co nanoparticles showed good dispersibility and loading capacity on the SiO_2 and carbon nanotube supports prepared in this study. The two as-prepared catalysts exhibited good catalytic activity and high stability, which indicates that SiO_2 and carbon nanotubes can be effectively applied as supports in F-T CO_2 hydrogenation.

References

[1] Bruce L., Takos J., Turney T. W., *ACS Symposium Series*, **1990**, *437*, 129

[2] Rodriguez Vallejo D. F., de Klerk A., *Energy & Fuels,* **2013**, *27*(6), 3137

[3] Fischer N., Clapham B., Feltes T., Claeys M., *ACS Catalysis,* **2015**, *5*(1), 113

[4] de Klerk A., de Vaal P. L., *Industrial & Engineering Chemistry Research.,* **2008**, *47*(18), 6870

[5] Dai Y. Y., Yu F., Li Z. J., An Y. L., Lin T. J., Yang Y. Z., Zhong L. S., Wang H., Sun Y. H., *Chinese Journal of Chemistry,* **2017**, *35*(6), 918

[6] Kibby C., Jothimurugesan K., Das T., Lacheen H. S., Rea T., Saxton R. J., *Catalysis Today,* **2013**, *215*, 131

[7] Arsalanfar M., Mirzaei A. A., Bozorgzadeh H. R., *Journal of Industrial and Engineering Chemistry*, **2013**, *19*(2), 478

[8] Khusnutdinova J. R., Garg J. A., Milstein D., *ACS Catalysis*, **2015**, *5*(4), 2416

[9] Xiang Y. Z., Chitry V., Liddicoat P., Felfer P., Cairney J., Ringer S., Kruse N., *Journal of the American Chemical Society,* **2013**, *135*(19), 7114

[10] Chen Y., Choi S., Thompson L. T., *ACS Catalysis,* **2015**, *5*(3), 1717

[11] Yang X. F., Kattel S., Senanayake S. D., Boscoboinik J. A., Nie X. W., Graciani J., Rodriguez J. A., Liu P., Stacchiola D. J., Chen J. G. G., *J. Am. Chem. Soc*., **2015**, *137*(32), 10104

[12] Zhang P., Tong J. L., Huang K., *ACS Sustainable Chemistry & Engineering*, **2016**, *4*(12), 7056

[13] Ma D. W., Niu S. T., Zhao J. L., Jiang X., Jiang Y. W., Zhang X. J., Sun T. M., *Chinese Journal of Chemistry,* **2017**, *35*(11), 1661

[14] Wang C. Z., Zhang Y., Wang Y. Z., Zhao Y. X., *Chinese Journal of Chemistry,* **2017**, *35*(1), 113

[15] Chang F. W., Hsiao T. J., Shih J. D., *Industrial & Engineering Chemistry Research,* **1998**, *37*(10), 3838

[16] Peng G. W., Sibener S. J., Schatz G. C., Ceyer S. T., Mavrikakis M., *Journal of Physical Chemistry C,* **2012**, *116*(4), 3001

[17] Hutschka F., Dedieu A., Eichberger M., Fornika. R., Leitner W., *J. Am. Chem. Soc.,* **1997**, *119*(19), 4432

[18] Theleritis D., Souentie S., Siokou A., Katsaounis A., Vayenas C. G., *ACS Catalysis,* **2012**, *2*(5), 770

[19] Fong H., Peters J. C., *Inorganic Chemistry,* **2015**, *54*(11), 5124

[20] Yu H. F., Liao P. Q., *Chem. Res. Chinese Universities,* **2016**, *32*(3), 390

[21] Spentzos A. Z., Barnes C. L., Bernskoetter W. H., *Inorganic Chemistry,* **2016**, *55*(16), 8225

[22] Liu H., Yang S. Z., Wang F., Bai C. X., Hu Y. M., Zhang X. Q., *Chin. J. Polym. Sci.,* **2016**, *34*(9), 1060

[23] Su B., Cao Z. C., Shi Z. J., *Accounts of Chemical Research,* **2015**, *48*(3), 886

[24] Melaet G., Ralston W. T., Li C. S., Alayoglu S., An K. J., Musselwhite N., Kalkan B., Somorjai G. A., *J. Am. Chem. Soc.,* **2014**, *136*(6), 2260

[25] Jeletic M. S., Helm M. L., Hulley E. B., Mock M. T., Appel A. M., Linehan J. C., *ACS Catalysis,* **2014**, *4*(10), 3755

[26] Grandjean D., Pelipenko V., Batyrev E. D., van den Heuvel J. C., Khassin A. A., Yurieva T. M., Weckhuysen B. M., *Journal of Physical Chemistry C*, **2011**, *115*(41), 20175

[27] Xu S. C., Walter E. D., Zhao Z. C., Hu M. Y., Han X. W., Hu J. Z., Bao X. H., *Journal of Physical Chemistry C.,* **2015**, *119*(36), 21219

[28] Kwak J. H., Kovarik L., Szanyi J., *ACS Catalysis,* **2013**, *3*(11), 2449

[29] Lwin S., Wachs I. E., *ACS Catalysis,* **2016**, *6*(1), 272

[30] Hu H., Cai S. X., Li H. R., Huang L., Shi L. Y., Zhang D. S., *ACS Catalysis,* **2015**, *5*(10), 6069

[31] Lu C. Q., Liu J. H., Jin C., Guo Y., Wang G. C., *Chem. Res. Chinese Universities,* **2017**, *33*(3), 406

[32] Xie H., Lu J. L., Shekhar M., Elam J. W., Delgass W. N., Ribeiro F. H., Weitz E., Poeppelmeier K. R., *ACS Catalysis,* **2013**, *3*(1), 61

[33] Samson K., Śliwa M., Socha R. P., Góra-Marek. K., Mucha D., Rutkowska-Zbik D., Paul J. F., Ruggiero-Mikołajczyk M., Grabowski R., Słoczyński J., *ACS Catalysis,* **2014**, *4*(10), 3730

[34] Zhang C. W., Xu L. B., Shan N. N., Sun T. T., Chen J. F., Yan Y. S., *ACS Catalysis,* **2014**, *4*(6), 1926

[35] Duan L. L., Fu R., Xiao Z. G., Zhao Q. F., Wang J. Q., Chen S. J., Wan Y., *ACS Catalysis,* **2015**, *5*(2), 575

[36] Li N., Wang X. M., Derrouiche S., Haller G. L., Pfefferle L. D., *ACS Nano.,* **2010**, *4*(3), 1759

[37] Pentsak E. O., Gordeev E. G., Ananikov V. P., *ACS Catalysis,* **2014**, *4*(11), 3806

[38] Chen Y., Chen H. R., Shi J. L., *Accounts of Chemical Research,* **2014**, *47*(1), 125

[39] Fu T., Cheng R. H., He X. L., Liu Z., Tian Z., Liu B. P., *Chin. J. Polym. Sci.,* **2017**, *35*(6), 739

[40] Lin X., Fu L. L., Chen Y., Zhu R. L., Wang S. Y., Liu Z. G., *ACS Applied Materials & Interfaces,* **2016**, *8*(40), 26809

[41] Guo T. Y., Du J. P., Wang S., Wu J. T., Li J. P., *Chem. Res. Chinese Universities*, **2016**, *32*(5), 843

[42] den Otter J. H., Nijveld S. R., de Jong K. P., *ACS Catalysis*, **2016**, *6*(3), 1616

[43] Vosoughi V., Badoga S., Dalai A. K., Abatzoglou N., *Industrial & Engineering Chemistry Research*, **2016**, *55*(21), 6049

[44] Fu T. J., Lv J., Li Z. H., *Industrial & Engineering Chemistry Research*, **2014**, *53*(4), 1342

[45] Kuo C. H., Li W. K., Song W. Q., Luo Z., Poyraz A. S., Guo Y., Ma A. W. K., Suib S. L., He J., *ACS Applied Materials & Interfaces*, **2014**, *6*(14), 11311

[46] Chen B., Chen J., Li J. Y., Tong X., Zhao H. C., Wang L. P., *Chin. J. Polym. Sci*., **2017**, *35*(3), 446

[47] Guo Y. L., Zhang R. Z., Wu K., Chen F., Fu Q., *Chin. J. Polym. Sci*., **2017**, *35*(12), 1497